PAPER

Tuning the spin-crossover properties of $Fe_4^{II}L_6$ cages *via* the interplay of coordination motif and linker modifications†

Tobias Paschelke,[a] Eicke Trumpf,[a] David Grantz, [ID][a] Malte Pankau,[a] Niclas Grocholski, [ID][a] Christian Näther, [ID][b] Frank D. Sönnichsen [ID][a] and Anna J. McConnell [ID]*‡[a]

Despite the increasing number of spin-crossover Fe[II]-based cages, the interplay between ligand modifications (*e.g.* coordination motif substituents and linker) is not well-understood in these multinuclear systems, limiting rational design. Here, we report a family of $Fe_4^{II}L_6$ spin-crossover cages based on 2,2′-pyridylbenzimidazoles where subtle ligand modifications lowered the spin crossover temperature in CD_3CN by up to 186 K. Comparing pairs of cages, CH_3 substituents on either the coordination motif or phenylene linker lowered the spin-crossover temperature by 48 K, 91 K or 186 K, attributed to electronic effects, steric effects and a combination of both, respectively. The understanding of the interplay between ligand modifications gained from this study could be harnessed on the path towards the improved rational design of spin-crossover cages.

Introduction

Most known spin-crossover complexes are based on Fe[II] ions.[1–5] These complexes can be switched between paramagnetic high- and diamagnetic low-spin states by external stimuli like light,[6–12] pressure[6,13,14] or temperature[6,10,15–20] if their spin-pairing and ligand field splitting energies are similar.[2,3,21] Despite extensive studies, there are still limitations to the prediction of spin-crossover properties[22] but methods have been established for predicting the spin state[23,24] and tuning the spin-crossover properties.[9,25] For example, steric bulk proximal to the coordination site is known to stabilize the high-spin state through lengthening the metal–ligands bonds.[26,27] However, rationalisation of electronic effects on the spin-crossover temperature ($T_{1/2}$) is more difficult, especially since most studies were performed in the solid state where intermolecular interactions also need to be considered.[18,28] Halcrow's systematic solution study on 2,6-di(pyrazol-1-yl)pyridine-based complexes revealed

that electron-donating *p*-pyridine substituents lower $T_{1/2}$ while *m*-pyrazole substituents raise it,[18] attributed to differing σ and π bonding contributions.[18,28]

Spin-crossover cages[29–39] consist of multiple Fe[II] ions and organic ligands with two or more coordination motifs connected *via* linkers. They are an interesting emerging class of spin-crossover materials[2,3] since multiple avenues exist for tuning the spin-crossover properties. These include modifications to the coordination motif,[31,36] guest encapsulation,[30,33,35] linker modifications[30] and cooperative effects. Furthermore, the potential to access multiple spin-states with distinct optical and magnetic properties makes cages appealing for applications as sensors, electronic switches and in information storage.[1–5]

However, spin-crossover cage examples, especially those studied in solution,[29,30,33,36,38] are limited and they are usually comprising imidazolimine ligands that form cubic[33,35,36,38,39] or tetrahedral[29–32,38] cages. The rational design of a cage with predictable spin-crossover properties is also challenging and the effect of modifications to the coordination motif and linker has not been extensively studied in Fe[II]-based cages.

Motivated to improve the rational design of spin-crossover cages, we studied a family of $Fe_4^{II}L_6$ cages (**1–11**, Fig. 1) and varied the coordination motif and linker to determine their influence on $T_{1/2}$. These subtle ligand modifications tuned the $T_{1/2}$ values, determined using the ideal solution model, from >430 K to 244 K in CD_3CN; $T_{1/2}$ decreased by 48 K from introducing CH_3 groups on the pyridine motifs (cage **6** *vs.* **10**), 91 K from increasing the steric bulk of the linker with CH_3

[a]Otto Diels Institute of Organic Chemistry, Kiel University, Otto-Hahn-Platz 4, Kiel 24098, Germany
[b]Institute of Inorganic Chemistry, Kiel University, Max-Eyth-Straße 2, Kiel 24118, Germany

‡Current address: Department of Chemistry and Biology, University of Siegen, Adolf-Reichwein-Strasse 2, Siegen 57068, Germany. E-mail: anna.mcconnell@uni-siegen.de
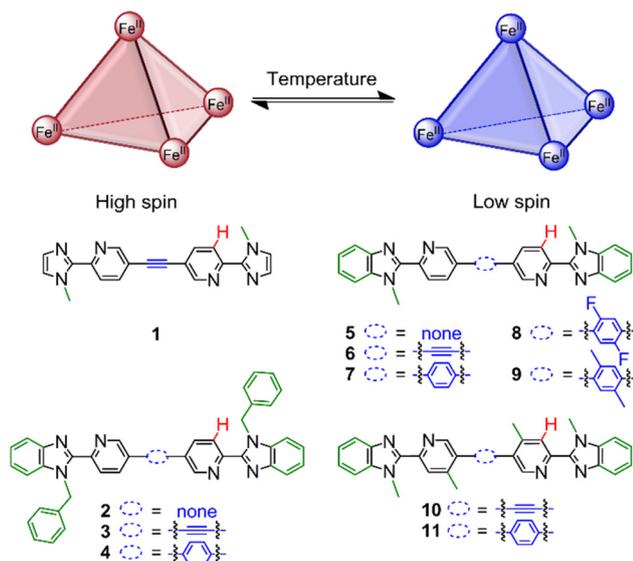
Fig. 1 Fe$^{II}_4$L$_6$ cages **1–11** for investigating the effect of ligand modifications within the coordination motif (represented by the changes in green) and linker (represented in blue) on the spin-crossover properties. The chemical shift changes of the proton in red were used for fitting to the ideal solution model.

groups (cage **7** *vs.* **9**) and 186 K for a combination of electronic and steric effects (cage **7** *vs.* **11**).

Results and discussion

Complexes and helicates based on 2,2′-pyridyl(benz)imidazole ligands exhibit a range of ligand field strengths, resulting in low-spin[40] complexes and those showing spin-crossover[41,42] depending on the ligand substitution. We decided to focus on Fe$^{II}_4$L$_6$ cages to probe the interplay of coordination site modifications and linker on $T_{1/2}$ since: (i) there are relatively few spin-crossover examples;[31,34,37] (ii) a variety of linkers can be introduced into the bis-bidentate ligand design with relative synthetic ease; (iii) the guest binding (*e.g.* solvent or counteranion) influence on $T_{1/2}$ is likely minimised by the more open faces of the cages as compared to the more enclosed faces of an Fe$^{II}_4$L$_4$ cage. The studies were performed in solution rather than the solid state to disentangle these intramolecular ligand field strength changes from intermolecular interactions. Furthermore, the structure and spin-state changes of individual species with temperature could be probed by NMR spectroscopy.

A family of Fe$^{II}_4$L$_6$ cages was designed based on four related coordination motifs with the modifications highlighted in green (Fig. 1): (i) imidazole-based **1** and benzimidazole-based (ii) **2–4** with *N*-benzyl substituents; (iii) **5–9** with *N*-methyl substituents; (iv) **10–11** with *N*-methyl substituents and CH$_3$ groups on the pyridine ring. Furthermore, the linker (Fig. 1, blue) was also varied from no spacer to an alkyne and phenylene derivatives. Edge-bridged Fe$^{II}_4$L$_6$ cages **1–11** (ESI, section 4†) were self-

assembled at room temperature in anhydrous acetonitrile in a glovebox using four equivalents of Fe(OTf)$_2$ and six equivalents of the appropriate ligand (preparations in ESI, section 2† using our recently reported one-pot Sonogashira-type procedure[43] or *via* Suzuki couplings). The corresponding Zn$^{II}_4$L$_6$ cages were also prepared using Zn(OTf)$_2$ to serve as diamagnetic analogues. However, a discrete cage species did not form with the imidazole ligand (ESI, section 3.1†).

The formation of M$_4$L$_6$ cages was confirmed by ESI mass spectrometry, the observation of one set of signals in the NMR spectra and in the case of cages **5** and **7**, by X-ray crystallography (Fig. 2 and ESI, section 6†). Although the diffraction data were of limited quality due to poor diffraction and disorder, as is commonly observed for metallosupramolecular cages,[44] they were sufficient to establish the cages' connectivity. In both cages, an *anti* ligand conformation was adopted resulting in a *T*-symmetric cage with the same stereochemistry at each metal center (Fig. 2). Cage **5** was also observed to bind a triflate counterion in its cavity.

While the Fe$^{II}_4$L$_6$ cages were obtained as the only species, a second minor species was also observed in some self-assemblies with Zn^{II} (ESI, sections 3.7, 3.8 and 3.10†). Analysis by ^{1}H and DOSY NMR spectroscopy and ESI mass spectrometry revealed the formation of Zn$_2$L$_3$ helicates. Lusby and co-workers have reported a helicate/tetrahedron equilibrium with the Co(II) and Co(III) analogues of cage **7**.[45] We attribute the formation of Zn$_2$L$_3$ but not Fe$_2$L$_3$ helicates to a combination of the metal's ionic radius and ligand's steric bulk increasing the energy of the Fe$_2$L$_3$ relative to the Fe$_4$L$_6$ self-assembly, as has been observed in related systems.[46,47]

The spin-crossover properties of cages **1–11** were investigated in solution between 248 K and 348 K in CD$_3$CN. While the Evans method[48] can determine the magnetic susceptibility from variable-temperature (VT) NMR experiments, preliminary
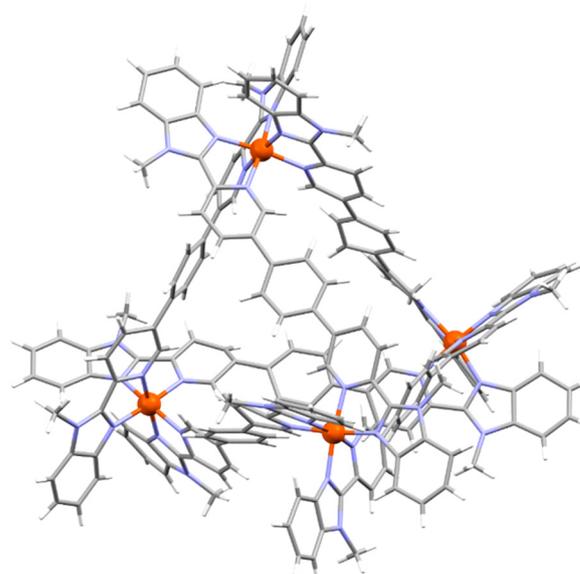

Fig. 2 X-ray crystal structure of cage **7**.

studies with cage **6** showed the NMR signals shifted upon addition of the *p*-xylene standard, suggesting possible guest binding (Fig. S239†). In addition, the magnetic susceptibility is dependent on accurate determination of the paramagnetic species concentration and influenced by the presence of other paramagnetic species, leading to large sources of error and inaccurate $T_{1/2}$ values.[49] Therefore, the ideal solution model[50] was used since the spin-crossover properties of a single species can be determined even in the presence of other paramagnetic impurities. In addition, our recent report of a paramagnetic NMR toolbox would enable the detailed characterisation of the cages in the high-spin state.[51] The chemical shift change of proton H (Fig. 1, red) was fitted using Origin (eqn (1)) to obtain ΔH, ΔS and $T_{1/2}$ values.§

$$\delta = \delta_{LS} + \frac{C}{T + T \cdot \exp\left(\dfrac{\Delta H - T\Delta S}{RT}\right)} \quad (1)$$

Only small chemical shift changes were observed for cages **1** and **2**, indicating that these cages are predominantly low spin over the measured temperature range (Fig. 3). For the other cages, initial fitting of all four parameters (C, ΔH, ΔS, δ_{LS}) resulted in large errors or the fitting did not converge (ESI, section 5†). Therefore, δ_{LS} was fixed to the chemical shift of the diamagnetic $Zn_4^{II}L_6$ cage analogue, yielding ΔH, ΔS and $T_{1/2}$ values for cages **6–11** (Table 1). The fitting for cages **3–5** still did not converge, likely attributable to an insufficient change in the spin-state populations within the temperature range available for the solvent CD_3CN.¶ Since cages **1–7** were predominantly low spin at 248 K, the magnitude of $\Delta\delta$ was used as a measure for $T_{1/2}$ in comparisons between cages where thermodynamic data could not be obtained.

One influence of the coordination motif on the spin-state can be delineated by comparing cages **1**, **3** and **6** (Fig. 3a). The increased $\Delta\delta$ values for benzimidazole-based cages **3** and **6** vs. diamagnetic imidazole-based cage **1** indicated the stabilization of the high-spin state, attributed to lengthening of the M–L bonds by the benzimidazole's steric bulk in **3** and **6** (Table 1).[40]

For benzimidazole-based cages **2–7** (Fig. 3b), the effect of *N*-benzylation was compared to *N*-methylation for three different linkers (alkyne, phenylene or no linker). Comparing cages with the same linker (*e.g.* **2** and **5**), larger $\Delta\delta$ values were observed for the *N*-methylated cages **5–7** than the *N*-benzylated analogues **2–4**, suggesting cages **5–7** have lower $T_{1/2}$ values.

§ This proton was chosen to allow comparison over the family of cages and for its proximity to the paramagnetic Fe[II] centres, resulting in large chemical shift changes without significant line broadening (relative to other protons) over the temperature range. For cages **9** and **11**, similar $T_{1/2}$ values were determined from fitting the chemical shift data for other protons close to the metal centre (ESI, sections 5.11 & 5.13†).

¶ In the Evans method, it is often possible to obtain $T_{1/2}$ values from data where there is a relatively small change of the spin-state fraction within the measured temperature range. This is because the maximum $\chi_m T$ value can be fixed to values reported in the literature for Fe(II) complexes during the fitting to the regular solution model. This is not possible in fitting data to the ideal solution model since the chemical shift of the high spin state (δ_{HS}) is not known.
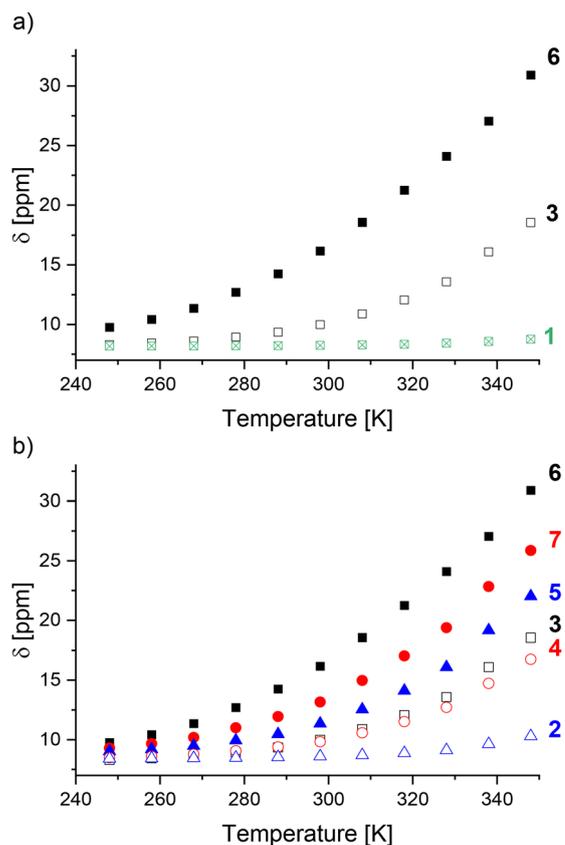

Fig. 3 Comparison of the chemical shift changes between 248 K and 348 K for cages: (a) **1**, **3** and **6**; (b) **2–7**. The symbol shading represents the change to the coordination motif: imidazole (⊠); *N*-benzylated benzimidazole (unfilled); *N*-methylated benzimidazole (filled). The symbol color and shape represent the linker: alkyne linker (black square); phenylene linker (red circle); no linker (blue triangle).

Table 1 Chemical shift changes and thermodynamic data from variable temperature NMR experiments

Cage	$\Delta\delta^a$ (ppm)	ΔH (kJ mol^{-1})	ΔS (J mol^{-1} K^{-1})	$T_{1/2}$ (K)
1	0.58	c	c	c
2	1.89	b	b	d
3	10.2	b	b	d
4	8.26	b	b	d
5	13.0	b	b	d
6	21.1	24.46 ± 0.58	60.94 ± 3.00	401
7	17.7	27.71 ± 0.91	64.48 ± 5.78	430
8	30.1	27.22 ± 0.93	72.61 ± 4.00	375
9	31.4	21.79 ± 0.48	64.32 ± 2.00	339
10	27.8	27.44 ± 1.12	77.65 ± 4.40	353
11	12.5	20.78 ± 0.22	85.05 ± 0.93	244

^{a} Based on the chemical shift change of proton H (red, Fig. 1) between 248 K and 348 K. ^{b} Could not be determined since fitting did not converge. ^{c} Low spin cage. ^{d} Proposed to be >430 K.

The linker's influence on the spin-crossover properties was also investigated. For both the *N*-methylated (**5–7**) and *N*-benzylated series (**2–4**), the largest $\Delta\delta$ values were observed for an alkyne followed by the phenylene and no linker

(Table 1). This was also reflected by the increasing $T_{1/2}$ values for the *N*-methylated cages: 401 K for cage **6** (alkyne linker), 430 K for cage **7** (phenylene linker) and >430 K for cage **5** (no linker).

Different factors were considered to explain the influence of the linker on $T_{1/2}$. First, the electronic effect of the linker was estimated using the Hammett parameter σ_m for C≡CH (0.21), C_6H_5 (0.06) and 3-pyridine (0.23).[52] However, their trend does not correlate with the observed $T_{1/2}$ trend. The Hammett parameters do not take into account electronic effects from metal complexation and these will be particularly significant for the cages without a linker as the 3-pyridine is part of the coordination motif.

The ligand conformation and mechanical coupling between the Fe^{II} centers could also play a role since the linkers' steric bulk dictates twisting within the ligand in order to adopt the required *anti* ligand conformation. Dihedral angles of approx. 10–22° for the phenylene linker and 50–65° for no linker were observed in the X-ray structures of cages **5**, **7** and related cages.[45,53] No cooperativity and weaker mechanical coupling is likely in cages with alkyne and phenylene linkers (**3–4**, **6–7**) given the large Fe^{II}–Fe^{II} distances (>13 Å in cage **7**) and ligand twisting, thus making spin-crossover more favorable.[38] In contrast, cages with no linkers (**2**, **5**) likely exhibit stronger mechanical coupling and cooperative effects cannot be excluded.

Finally, the cavity size as dictated by the ligand length could also influence $T_{1/2}$ *via* host–guest chemistry. While the same counteranion OTf⁻ was used for all cages to minimize guest binding effects, the smallest cages **3** and **5** were observed to bind the counterion in slow exchange by ^{19}F NMR spectroscopy (Fig. S174 and S195†) and in the case of **5**, in the X-ray crystal structure (Fig. S293†).

While these different factors were considered, it was not possible to rationalize the observed $T_{1/2}$ trend as a function of the linker. Therefore, to gain further insight into coordination site and linker modifications on $T_{1/2}$, sets of cages (**6** and **10**, **7–9**, **7** and **11**) with the same ligand scaffold but minor modifications (*e.g.* a F or CH_3 substituent) were compared. Given the larger size of cages **7–11** and the observation of fast exchange of the counterion OTf⁻ in the ^{19}F NMR spectra at room temperature (Fig. S208, S215, S223, S230 and S236†), it was hypothesised that ligand field strength effects would dominate over solvent, guest binding and ion-pairing effects enabling the determination of trends based on steric and electronic effects.

As a control, anion binding experiments (ESI, section 7†) were carried out with cages **7** and **11** since this set of cages displayed the largest $T_{1/2}$ change within this study (Table 1). To probe guest binding within the cavity, 8 equivalents (relative to the cage) of the smaller counterion BF_4^- were added to each cage and the broad ^{19}F signals for BF_4^- indicated fast guest exchange (Fig. S296 and S299†). Small chemical shift changes ($\Delta\delta < 0.2$ ppm) were observed in the ^1H NMR spectra and the insignificant changes of the phenylene protons ($\Delta\delta < 0.05$ ppm) suggested counteranion binding in the cavity has a minimal effect (Fig. S295 and S297†).

Further experiments with cage **7** focused on ion-pairing. NTf_2^- was chosen as a counterion since the sharp signal in the ^{19}F NMR spectrum suggested that it is too large to fit in the cavity (Fig. S303†). Again, small ^1H chemical shift changes were observed, meaning ion-pairing likely has an insignificant effect on $T_{1/2}$. Finally, VT NMR experiments with cages **7** and **11** in the presence and absence of competing counteranions showed no evidence of a change from fast to slow counteranion exchange upon cooling to 248 K due to increased population of the low spin state with a smaller cavity (Fig. S297–S304†). Based on these control experiment results, the effect of ion-pairing or guest binding on the spin-crossover properties is proposed to be negligible for comparisons within a set of cages.

Cages **7–9** were compared where F or CH_3 substituents were introduced on the phenylene linker to increase the steric bulk without changing the ligand length. $T_{1/2}$ decreased from 430 K (cage **7**) to 375 K for cage **8** with F substituents and to 339 K for cage **9** with CH_3 substituents (Table 1). While the high-spin fraction of cage **7** at 298 K is 3%, increasing high-spin-state populations of 10% and 26% were obtained for cages **8–9**, respectively (Fig. 4). Thus, $T_{1/2}$ decreases with increasing substituent size on the linker, attributed to increased dihedral angles between the coordination motif and the linker, as observed in crystal structures of related cages.[45] However, contributions from electronic effects cannot be completely neglected since CH_3 groups are electron-donating, while F is electron-withdrawing.

Thermodynamic data analysis revealed cages **7** and **8** have similar enthalpies but cage **8** has an increased entropy (Table 1). In contrast, cage **9** had a lower enthalpy compared to cage **7**, but the entropy values were similar. Thus, the spin-transition of cage **9** is enthalpically driven, while for cage **8** it is entropically controlled. It is difficult to draw conclusions from these data since the relationship between both energies
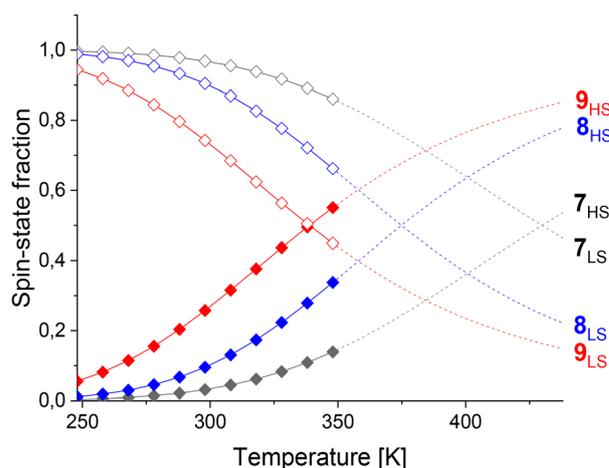

Fig. 4 High (filled diamonds) and low (unfilled diamonds) spin-state fractions of cages **7** (black), **8** (blue) and **9** (red) from VT NMR measurements between 248 K and 348 K. Data above 348 K (dashed lines) was extrapolated.

on spin-crossover properties has not been systematically studied.[54] However, we attribute stabilization of the high-spin state for cage **9** *vs.* cage **7** to the increased dihedral angles from the steric bulk of the CH_3 groups and the required adoption of an *anti*-conformation, leading to weakened M–L bonds. Thus, modifications through CH_3 substituents on the phenylene linker tuned $T_{1/2}$ by 91 K.

Further coordination site modifications were introduced to investigate the influence of interactions between these and the linker on $T_{1/2}$. For example, Halcrow and co-workers have shown that electron-donating groups on *para*-substituted pyridines in Fe^{II} mononuclear complexes based on 2,6-bis(pyrazol-1-yl)pyridines can stabilize the high-spin state.[18] Therefore, CH_3 groups were introduced on the pyridine motif in cages **10** and **11** in an attempt to decrease $T_{1/2}$ towards room temperature. Comparing cages **6** and **10**, the introduction of the CH_3 groups decreased $T_{1/2}$ from 401 K to 353 K (Table 1), resulting in an increase of the high-spin state fraction at 298 K from 7% to 15% (Fig. 5). We propose the stabilization of the high-spin state by 48 K is largely due to electronic effects since steric effects from the alkyne linker are minimized.

Surprisingly, $T_{1/2}$ decreased by 186 K from 430 K to 244 K for cage **7** *vs.* **11** (Table 1). The introduction of a CH_3 group in cage **11** yields a largely high-spin cage (86% high-spin state fraction) at 298 K, while cage **7** is almost completely low-spin (3% high-spin state fraction) (Fig. 5). We attribute this large change to electronic effects, and moreover, to strong steric clashes between the CH_3 substituents and the phenylene linker in cage **11**, increasing the dihedral angles between the linker and the pyridine rings as observed in crystal structures of related cages.[55] Comparing thermodynamic data (Table 1), both the enthalpy and entropy increased for cage **10** *vs.* **6**. Although the increased entropy favors the high-spin state, this is partly counteracted by the increased enthalpy stabilizing the low-spin state, resulting in a smaller $T_{1/2}$ difference. In contrast, the decrease of the enthalpy and increase of the entropy for cage **11** *vs.* **7** both favor the high-spin state, leading to the larger $T_{1/2}$ change of 186 K.

Conclusions

This study demonstrates the power of solution-based spin-crossover studies using the ideal solution model for quantifying ligand field strength modifications in the absence of intermolecular interactions, as exemplified in this family of $Fe_4^{II}L_6$ cages. Furthermore, information about the cage's structure and spin-state can be obtained from VT NMR experiments independently of other paramagnetic species.

Imidazole-based cage **1** was low-spin over the measured temperature range. However, the steric bulk of the benzimidazole motif in cages **2**–**11** stabilized the high-spin state.

While substitution of the coordination motif is known to influence $T_{1/2}$ in spin-crossover complexes, this systematic study reveals that the linker can also have a profound effect, despite the increased distance from the metal centers. Importantly, the interplay of coordination site and linker modification effects was quantified and minor modifications like the introduction of CH_3 groups tuned $T_{1/2}$ by up to 186 K. *p*-CH_3 substituents on the pyridine motif decreased $T_{1/2}$ by 48 K for cage **10** *vs.* **6** with alkyne linkers, attributed to predominantly electronic effects. CH_3 substituents on the phenylene linker decreased $T_{1/2}$ by 91 K for cage **9** *vs.* **7**, largely attributed to steric clashes. Finally, a combination of both effects is proposed to result in the 186 K $T_{1/2}$ decrease in cage **11** *vs.* **7** due to both electronic effects from the *p*-CH_3 substituents on the pyridine and a steric clash with the phenylene linker.

Thus, this study demonstrates how seemingly subtle modifications (*i.e.* substitution of H for CH_3) can significantly impact the spin-crossover properties of multinuclear Fe^{II}-based cages in solution, resulting in large $T_{1/2}$ changes of almost 200 K and altering the spin state from predominantly low spin to high spin at room temperature. Future work will investigate how this understanding of the interplay between ligand modifications can be applied to the design of spin-crossover cages with more predictable spin-crossover pro-
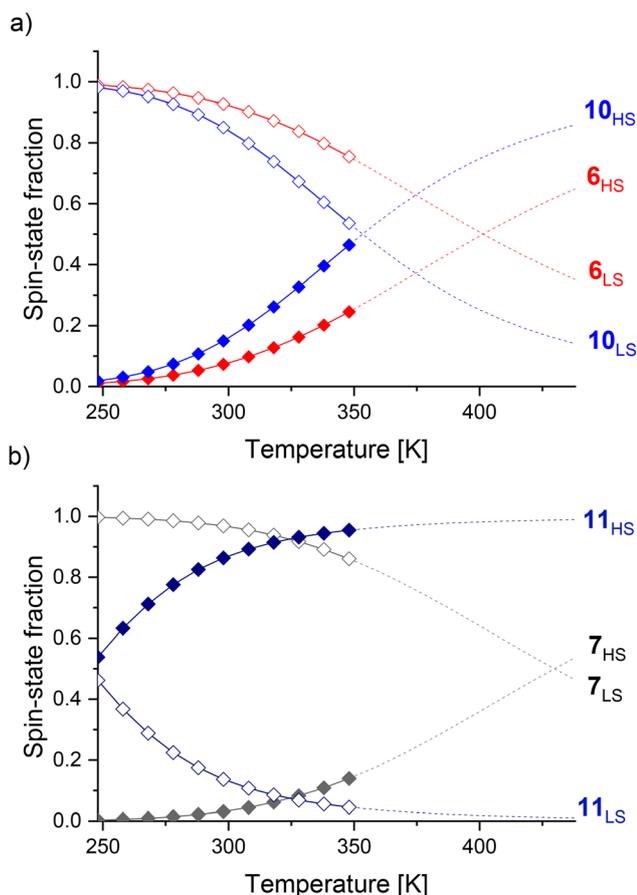

Fig. 5 High (filled diamonds) and low (unfilled diamonds) spin-state fractions of cages: (a) **6** (red) and **10** (blue); (b) **7** (grey) and **11** (blue) from VT NMR measurements between 248 K and 348 K. Data above 348 K (dashed lines) was extrapolated.

perties. This would facilitate the tailored application of spin-crossover cages, *e.g.* as sensors.

Author contributions

T. P.: conceptualisation (lead), data curation (lead), formal analysis (lead), investigation (lead), resources (lead), supervision (supporting), visualisation (lead), writing-original draft (lead), writing-review and editing (equal). E. T.: conceptualisation (lead), formal analysis (supporting), investigation (supporting), resources (supporting), visualisation (lead), writing-original draft (supporting), writing-review and editing (equal). D. G.: formal analysis (supporting), investigation (supporting), resources (supporting), writing-review and editing (supporting). M. P.: formal analysis (supporting), investigation (supporting), resources (supporting), visualisation (supporting), writing-review and editing (supporting). N. G.: formal analysis (supporting), investigation (supporting), resources (supporting), writing-review and editing (supporting). C. N.: formal analysis (supporting), investigation (supporting), resources (supporting), writing-review and editing (supporting). F. D. S.: investigation (supporting), methodology (lead), resources (supporting), writing-review and editing (equal). A. J. M.: conceptualisation (lead), formal analysis (supporting), funding acquisition (lead), project administration (lead), supervision (lead), writing-original draft (supporting), writing-review and editing (equal).

Conflicts of interest

There are no conflicts to declare.

Acknowledgements

References

1 M. A. Halcrow, *Chem. Soc. Rev.*, 2011, **40**, 4119–4142.

2 A. J. McConnell, *Supramol. Chem.*, 2018, **30**, 858–868.

3 R. W. Hogue, S. Singh and S. Brooker, *Chem. Soc. Rev.*, 2018, **47**, 7303–7338.

4 H. S. Scott, R. W. Staniland and P. E. Kruger, *Coord. Chem. Rev.*, 2018, **362**, 24–43.

5 W. Huang, X. Ma, O. Sato and D. Wu, *Chem. Soc. Rev.*, 2021, **50**, 6832–6870.

6 E. Breuning, M. Ruben, J.-M. Lehn, F. Renz, Y. Garcia, V. Ksenofontov, P. Gütlich, E. Wegelius and K. Rissanen, *Angew. Chem., Int. Ed.*, 2000, **39**, 2504–2507.

7 T. Matsumoto, G. N. Newton, T. Shiga, S. Hayami, Y. Matsui, H. Okamoto, R. Kumai, Y. Murakami and H. Oshio, *Nat. Commun.*, 2014, **5**, 3865.

8 B. Rösner, M. Milek, A. Witt, B. Gobaut, P. Torelli, R. H. Fink and M. M. Khusniyarov, *Angew. Chem., Int. Ed.*, 2015, **54**, 12976–12980.

9 M. Mörtel, A. Witt, F. W. Heinemann, S. Bochmann, J. Bachmann and M. M. Khusniyarov, *Inorg. Chem.*, 2017, **56**, 13174–13186.

10 T. Shiga, G. N. Newton and H. Oshio, *Dalton Trans.*, 2018, **47**, 7384–7394.

11 H.-Y. Sun, Y.-S. Meng and T. Liu, *Chem. Commun.*, 2019, **55**, 8359–8373.

12 M. Oppermann, F. Zinna, J. Lacour and M. Chergui, *Nat. Chem.*, 2022, **14**, 739–745.

13 D. C. Fisher and H. G. Drickamer, *J. Chem. Phys.*, 1971, **54**, 4825–4837.

14 R. J. Butcher, J. R. Ferraro and E. Sinn, *Inorg. Chem.*, 1976, **15**, 2077–2079.

15 J. Elhaïk, V. A. Money, S. A. Barrett, C. A. Kilner, I. R. Evans and M. A. Halcrow, *Dalton Trans.*, 2003, 2053–2060.

16 B. Schneider, S. Demeshko, S. Dechert and F. Meyer, *Angew. Chem., Int. Ed.*, 2010, **49**, 9274–9277.

17 S. Chorazy, R. Podgajny, K. Nakabayashi, J. Stanek, M. Rams, B. Sieklucka and S.-i. Ohkoshi, *Angew. Chem., Int. Ed.*, 2015, **54**, 5093–5097.

18 L. J. K. Cook, R. Kulmaczewski, R. Mohammed, S. Dudley, S. A. Barrett, M. A. Little, R. J. Deeth and M. A. Halcrow, *Angew. Chem., Int. Ed.*, 2016, **55**, 4327–4331.

19 A. A. Pavlov, G. L. Denisov, M. A. Kiskin, Y. V. Nelyubina and V. V. Novikov, *Inorg. Chem.*, 2017, **56**, 14759–14762.

20 S. Chorazy, J. J. Stanek, J. Kobylarczyk, S.-i. Ohkoshi, B. Sieklucka and R. Podgajny, *Dalton Trans.*, 2017, **46**, 8027–8036.

21 C.-M. Jureschi, J. Linares, A. Boulmaali, P. R. Dahoo, A. Rotaru and Y. Garcia, *Sensors*, 2016, **16**, 187.

22 N. Deorukhkar, C. Besnard, L. Guénée and C. Piguet, *Dalton Trans.*, 2021, **50**, 1206–1223.

23 H. Phan, J. J. Hrudka, D. Igimbayeva, L. M. L. Daku and M. Shatruk, *J. Am. Chem. Soc.*, 2017, **139**, 6437–6447.

24 S. Rodríguez-Jiménez, M. Yang, I. Stewart, A. L. Garden and S. Brooker, *J. Am. Chem. Soc.*, 2017, **139**, 18392–18396.

25 D. Y. Aleshin, I. Nikovskiy, V. V. Novikov, A. V. Polezhaev, E. K. Melnikova and Y. V. Nelyubina, *ACS Omega*, 2021, **6**, 33111–33121.

26 H. A. Goodwin, E. S. Kucharski and A. H. White, *Aust. J. Chem.*, 1983, **36**, 1115–1124.

27 C. Bartual-Murgui, S. Vela, M. Darawsheh, R. Diego, S. J. Teat, O. Roubeau and G. Aromí, *Inorg. Chem. Front.*, 2017, **4**, 1374–1383.

28 L. Bondì, A. L. Garden, F. Totti, P. Jerabek and S. Brooker, *Chem. – Eur. J.*, 2022, **28**, e202104314.

29 A. Ferguson, M. A. Squire, D. Siretanu, D. Mitcov, C. Mathonière, R. Clérac and P. E. Kruger, *Chem. Commun.*, 2013, **49**, 1597–1599.

30 R. A. Bilbeisi, S. Zarra, H. L. C. Feltham, D. N. L. Jameson, J. K. Clegg, S. Brooker and J. R. Nitschke, *Chem. – Eur. J.*, 2013, **19**, 8058–8062.

31 D.-H. Ren, D. Qiu, C.-Y. Pang, Z. Li and Z.-G. Gu, *Chem. Commun.*, 2015, **51**, 788–791.

32 L. Li, N. Saigo, Y. Zhang, D. J. Fanna, N. D. Shepherd, J. K. Clegg, R. Zheng, S. Hayami, L. F. Lindoy, J. R. Aldrich-Wright, C.-G. Li, J. K. Reynolds, D. G. Harman and F. Li, *J. Mater. Chem. C*, 2015, **3**, 7878–7882.

33 N. Struch, C. Bannwarth, T. K. Ronson, Y. Lorenz, B. Mienert, N. Wagner, M. Engeser, E. Bill, R. Puttreddy, K. Rissanen, J. Beck, S. Grimme, J. R. Nitschke and A. Lützen, *Angew. Chem., Int. Ed.*, 2017, **56**, 4930–4935.

34 L. Li, A. R. Craze, O. Mustonen, H. Zenno, J. J. Whittaker, S. Hayami, L. F. Lindoy, C. E. Marjo, J. K. Clegg, J. R. Aldrich-Wright and F. Li, *Dalton Trans.*, 2019, **48**, 9935–9938.

35 H.-S. Lu, W.-K. Han, X. Yan, Y.-X. Xu, H.-X. Zhang, T. Li, Y. Gong, Q.-T. Hu and Z.-G. Gu, *Dalton Trans.*, 2020, **49**, 4220–4224.

36 M. Hardy, J. Tessarolo, J. J. Holstein, N. Struch, N. Wagner, R. Weisbarth, M. Engeser, J. Beck, S. Horiuchi, G. H. Clever and A. Lützen, *Angew. Chem., Int. Ed.*, 2021, **60**, 22562–22569.

37 W. Li, C. Liu, J. Kfoury, J. Oláh, K. Robeyns, M. L. Singleton, S. Demeshko, F. Meyer and Y. Garcia, *Chem. Commun.*, 2022, **58**, 11653–11656.

38 J. Zheng, L. K. S. von Krbek, T. K. Ronson and J. R. Nitschke, *Angew. Chem., Int. Ed.*, 2022, **61**, e202212634.

39 H. Min, A. R. Craze, M. J. Wallis, R. Tokunaga, T. Taira, Y. Hirai, M. M. Bhadbhade, D. J. Fanna, C. E. Marjo, S. Hayami, L. F. Lindoy and F. Li, *Chem. – Eur. J.*, 2023, **29**, e202203742.

40 K. H. Sugiyarto and H. A. Goodwin, *Aust. J. Chem.*, 1987, **40**, 775–783.

41 S. G. Telfer, B. Bocquet and A. F. Williams, *Inorg. Chem.*, 2001, **40**, 4818–4820.

42 T. Lathion, L. Guénée, C. Besnard, A. Bousseksou and C. Piguet, *Chem. – Eur. J.*, 2018, **24**, 16873–16888.

43 M. Lehr, T. Paschelke, V. Bendt, A. Petersen, L. Pietsch, P. Harders and A. J. McConnell, *Eur. J. Org. Chem.*, 2021, 2728–2735.

44 K. Rissanen, *Chem. Soc. Rev.*, 2017, **46**, 2638–2648.

45 M. J. Burke, G. S. Nichol and P. J. Lusby, *J. Am. Chem. Soc.*, 2016, **138**, 9308–9315.

46 R. G. Siddique, K. S. A. Arachchige, H. A. Al-Fayaad, J. C. McMurtrie and J. K. Clegg, *Dalton Trans.*, 2022, **51**, 12704–12708.

47 Q. Shi, X. Zhou, W. Yuan, X. Su, A. Neniškis, X. Wei, L. Taujenis, G. Snarskis, J. S. Ward, K. Rissanen, J. de Mendoza and E. Orentas, *J. Am. Chem. Soc.*, 2020, **142**, 3658–3670.

48 D. F. Evans, *J. Chem. Soc.*, 1959, 2003–2005.

49 S. De, S. Tewary, D. Garnier, Y. Li, G. Gontard, L. Lisnard, A. Flambard, F. Breher, M.-L. Boillot, G. Rajaraman and R. Lescouëzec, *Eur. J. Inorg. Chem.*, 2018, **2018**, 414–428.

50 W. Kläui, W. Eberspach and P. Gütlich, *Inorg. Chem.*, 1987, **26**, 3977–3982.

51 M. Lehr, T. Paschelke, E. Trumpf, A.-M. Vogt, C. Näther, F. D. Sönnichsen and A. J. McConnell, *Angew. Chem., Int. Ed.*, 2020, **59**, 19344–19351.

52 C. Hansch, A. Leo and R. W. Taft, *Chem. Rev.*, 1991, **91**, 165–195.

53 N. Ousaka, J. K. Clegg and J. R. Nitschke, *Angew. Chem., Int. Ed.*, 2012, **51**, 1464–1468.

54 K. P. Kepp, *Inorg. Chem.*, 2016, **55**, 2717–2727.

55 W. Meng, J. K. Clegg, J. D. Thoburn and J. R. Nitschke, *J. Am. Chem. Soc.*, 2011, **133**, 13652–13660.